Mathematical Modelling and Numerical Simulation with Applications, 2025, 5(1), 97–116

https://dergipark.org.tr/en/pub/mmnsa
ISSN Online: 2791-8564 / Open Access
https://doi.org/10.53391/mmnsa.1522021

RESEARCH PAPER

Numerical analysis of the three-dimensional model of pulsatile and non-Newtonian blood flow in a carotid artery with local occlusion

Mansur Mustafaoğlu [1,‡], **İsak Kotçioğlu** [1,‡] **and Muhammet Kaan Yeşilyurt** [1,*,‡]

[1]Department of Mechanical Engineering, Faculty of Engineering, Ataturk University, 25240 Erzurum, Türkiye

*Corresponding Author
‡mansour@atauni.edu.tr (Mansur Mustafaoğlu); ikotcioglu@atauni.edu.tr (İsak Kotçioğlu); kaan.yesilyurt@atauni.edu.tr (Muhammet Kaan Yeşilyurt)

Abstract

The analysis of blood flow in blood vessels, particularly in arteries, is a topic with important clinical applications. The blood can undergo a reduction in its viscosity under shear stress, which is called shear thinning. In this study, the effect of the shear thinning of blood is simulated using the Carreau-Yasuda model, neglecting the viscoelastic effects. The purpose of this investigation is to analyze the pulsatile blood flow in a three-dimensional model of the carotid artery and the effects of occlusion using Ansys Fluent. The results obtained in this study show that, compared to Newtonian fluids, non-Newtonian fluids exhibit significant differences in secondary flow patterns and shear flow behavior. Additionally, the axial velocity in the non-planar branch decreases with obstruction. The maximum shear stress of the walls with Newtonian fluid viscosity exhibits a significant error, and the values are lower than those of walls with non-Newtonian viscosity in most cases. In continuation of this research, vessel occlusion models with different occlusion sizes are analyzed. In the case where the outlet of the vessel is narrowed, an increase in velocity is observed in the furcation area. Although the software cannot simulate rupture, occlusion of the vessel at 80% and 50% of the internal diameter is analyzed.

Keywords: Non-Newtonian fluid; shear thinning; Carreau-Yasuda model; blood flow; CFD analysis

AMS 2020 Classification: 65N12; 76A05; 92C35

1 Introduction

Cardiovascular diseases (CVDs) account for approximately 17.9 million deaths annually, which corresponds to 32% of all global deaths. Including coronary artery disease, stroke, and hypertension, CVDs are often linked to abnormalities in blood flow and vessel occlusion. Besides being the

➤ **Received:** 25.07.2024 ➤ **Revised:** 11.02.2025 ➤ **Accepted:** 16.02.2025 ➤ **Published:** 31.03.2025

leading cause of death globally, CVDs also create a significant economic burden, with healthcare costs and productivity losses estimated to exceed one trillion US dollars annually worldwide. Understanding the hemodynamics of blood flow, particularly in occluded vessels, is therefore critical for developing effective diagnostic and therapeutic strategies against CVDs.

With the increasing number of CVDs during the last few decades, the study of blood flow in vessels and its behavior has been of particular importance and interest. Through a review of the literature, it has become clear that there is still much to investigate regarding the shear stress on the walls of the vessels, the effects of the hyperelasticity of the blood vessels, and how blood interacts with the vessel structure under different gravity conditions. Another CVD, carotid artery disease, is a condition characterized by the narrowing of the carotid arteries, the primary vessels supplying oxygenated blood to the brain. This narrowing, or stenosis, is typically caused by the accumulation of atherosclerotic plaque within the arterial walls. The primary objective of treatment is to mitigate the risk of ischemic stroke by reducing plaque burden, preventing thrombus formation, and maintaining adequate cerebral blood flow. Currently, it has been proven that the occurrence of many CVDs is linked to blood flow characteristics [1].

Blood is a concentrated suspension of red blood cells (RBCs) in plasma, with these cells constituting nearly 45% of the total blood volume. At normal temperatures, blood behaves as non-Newtonian in the form of shear liquefaction [2]. A cramp is an abnormal swelling in a vein or other organs with tubular structures in the body. Sometimes, it is also called stenosis [3] and [4]. From the point of view of fluid mechanics, constriction indicates the presence of an obstacle to blood flow inside the vessel [5]. Vascular branches in areas that have abnormal fluid dynamics are known to be prone to atherosclerosis. Fluid mechanics studies have shown that atherosclerosis occurs at bifurcations that have a complex geometry, i.e., in areas with a high Reynolds number and where the shear stress is lower than the average of wall shear stress (WSS). The curvature of the wall is related; in addition, local disturbances and areas of circulation play important roles in the initiation and development of atherosclerosis. It is thought that the complexity of the blood flow dynamics downstream of the occlusion will cause further development of the occlusion or cause the plaque to be vulnerable to failure and thrombosis. It is almost universally accepted that blood vessels that have curves or bifurcations are prone to constriction due to the complexity of the flow in these areas [6]. Because the blood flow is pulsatile, these complicated flow patterns cause constrictions in certain periods within the geometries that feature high shear stress, separation, circulation, and turbulent flow.

Various studies have been conducted in this field. The investigation of blood flow in narrowed vessels is an interesting topic that has attracted the attention of many researchers. This issue is particularly important because the blood flow in constricted vessels and channels has a crucial impact on the development of vascular obstruction [7]. Examining the mechanism of blood flow and the distribution of blood flow in these stages leads to determining the dependence of blood flow on various physical and physiological factors and to a correct understanding of this phenomenon. As a result, it is possible to solve this problem or prevent it from an engineering point of view. As a result of the clogging and narrowing (obstruction) that occur in the vein, the normal flow of blood is disrupted. This disturbance in normal blood flow plays an important role in vascular diseases. For this reason, to determine how constriction affects blood flow and analyze blood flow in the parts of vessels that are clogged or blocked, much research has been performed, including laboratory investigations as well as numerical studies.

Having started approximately 25 years ago, several experimental research studies have been conducted using different laboratory models to study how unstable flow affects the blood flow at occlusion sites. With the advancement of computational methods in recent years, later studies featuring numerical simulations of this physiological phenomenon have been performed by

numerous researchers [8, 9]. Many researchers have studied pulsatile blood flow in healthy and blocked vessels using computational fluid dynamics (CFD) and compared the results using MRI techniques [7, 10, 11].

Clogged or engorged blood vessels face various hemodynamic consequences of pressure drop, which lead to the development of clots. The pressure drop depends on the flow velocity and the geometry of the constriction, but the properties of fluid, such as density and apparent viscosity, are relatively constant. Multiple constrictions in the arteries are the result of plaque growth in atherosclerosis, which can collapse under certain physiological conditions [5].

Vascular narrowing is often accompanied by an unusual sound of blood flow, which results from the disturbance of flow in the narrowed channel, and in this way, the location of the constriction can be recognized. These sounds can be heard using a medical stethoscope, but disease diagnosis with medical imaging refers to the set of methods and techniques that can be used to obtain visual images of the parts of the human body [12].

Seo [13] investigated blood flow in the human carotid artery using ANSYS software. He investigated the effect of the interaction between fluid and solid on the flow characteristics and shear stress of the wall. He investigated two flow models, one of which considered the interaction between solid and fluid, while the other did not. The results showed that the shear stress values for these two models differ between 5% and 11%.

The collapse of the inner wall of the vessel is a process in which the bending of the artery is under certain pressure and tension, and under these conditions, the collapse of the inner wall of the vessel occurs. The result of the compression resulting from this collapse is to speed up the process of fatigue and rupture. If plaque detachment occurs in the coronary and cerebral arteries, it directly leads to a heart attack or stroke. The activity of blood plaques in certain cases, such as cramps and, in particular, when thrombosis occurs, is of great interest [6]. Upon plaques sticking together, congestion develops, and once the flow becomes sufficiently constricted, turbulence may increase, bringing on an increase in the shear stress of the flow and the walls. Studies in the computer environment show that flow transitions into turbulent and back into laminar in pulsatile flow; therefore, it is very important to predict transient and turbulent flow in flows with low Reynolds numbers when simulating blood flow within blood vessels with occlusion [14]. Another factor that affects blood viscosity is the concentration and type of proteins in plasma, but these effects are so small that they are not considered important in most hemodynamic studies [15].

Using Ansys software, Dong et al. [16] conducted a numerical study to explore the relationship between mechanical forces that are exerted at the coronary branching (furcation) sites and the angle of furcation, considering the division angles to be between 75 and 120 degrees. The results revealed a relationship between environmental stress and left coronary artery diseases. In addition, they considered two elastic and nonelastic assumptions for the blood vessel [16]. On the other hand, Leeuwen et al. [17] investigated the diameter of the vessel and the RBC velocity in the vessel and reported that vessel constriction induces a large change in the RBC velocity [17].

Botti et al. [18] conducted a CFD study modeling the blood hemodynamics of a specific patient with an intracranial aneurysm by using two different CFD solvers, i.e., the finite element method and the finite volume method, in order to compare their performances. They reported that the finite element model provided better accuracy in high-order analysis for every degree of freedom [18].

The particle hydrodynamic method has always been developed as a meshless Lagrange method for simulating fluid-structure interactions. This algorithm, which involves the two-dimensional simulation of blood flow, provides new support for the application of the SPH method. This method is used to simulate the opening of the elastic valve due to the force of the fluid column behind it, which, compared to the experimental results, proves the ability of this method to solve

fluid and structural problems [19].

Many of the studies reported in the literature have focused on Newtonian fluid models or simplified geometries. While some have incorporated non-Newtonian models, they often neglect the effects of pulsatile flow or fail to analyze the impact of varying occlusion sizes on flow patterns and wall shear stress. This study aims to address these gaps by employing a non-Newtonian Carreau-Yasuda model to simulate pulsatile blood flow in a three-dimensional model of the carotid artery with varying degrees of occlusion. By incorporating realistic vessel geometry and pulsatile flow conditions, this study provides a more accurate representation of the hemodynamics in stenotic vessels. Furthermore, the analysis of different occlusion sizes (50% and 80% of the internal diameter) is important to address in more detail the hemodynamic risks associated with high occlusion levels and their implications for CVDs.

The purpose of this study was to analyze the pulsatile flow inside vessels with non-Newtonian blood fluid. In the present study, the flow is unsteady and fully developed before entry. The Carreau model is considered for the simulation of non-Newtonian blood fluid. Additionally, the values of velocity and pressure are defined the same as real values and with pulses.

2 Materials and methods

This section presents the governing flow equations and the corresponding boundary conditions. Homogeneous fluid motion equations are derived from the conservation principles of mass, momentum, and energy. To facilitate engineering analysis, a continuum assumption is employed, averaging the fluid properties over a representative elementary volume. This assumption is called continuous media, and as long as the smallest physical dimension is much larger than the free distance of molecules, this assumption is true.

Another assumption made in this study is that the blood was an incompressible fluid. This assumption is justified by the fact that the density of blood remains nearly constant under physiological conditions. The compressibility of blood is negligible due to the fact that the greatest part of the blood plasma, as high as 90%, consists of water and that the pressure variations in the cardiovascular system is relatively low. This assumption simplifies the continuity equation and is consistent with the majority of blood flow models in the literature.

Governing equations

The governing equations are for the solid wall that interacts with the fluid. The equations solved in the ANSYS software include the equations of conservation of mass Eq. (1) and momentum Eq. (2).

$$\frac{\partial p}{\partial t} + \nabla \cdot (\rho V) = 0. \tag{1}$$

The momentum equations, also known as the Navier–Stokes equations, govern viscous flow of Newtonian fluids and can be written as in Eq. (2) in the general form:

$$\rho \left(\frac{\partial u_i}{\partial t} + \mathbf{u_j} \frac{\partial u_i}{\partial x_j} \right) = \frac{\partial P}{\partial x_j} + \mathbf{B_i} + \frac{\partial}{\partial x_i} \left[\mu \left(\frac{\partial u_i}{\partial x_j} + \frac{\partial u_j}{\partial x_i} - \frac{2}{3} \mathbf{‹_{ij}} \frac{\partial u_k}{\partial x_k} \right) \right], \tag{2}$$

where B_i represents the body forces that include primarily the gravitational forces, which are relevant in hemodynamic studies. Other body forces, such as electromagnetic forces, are mostly irrelevant and, therefore, negligible in this context.

This method can usually remove the viscosity of the fluid from inside the derivative, and in the

Table 1. Constant values of the k-ω turbulence model

σ_ω	σ_k	$'\beta$	β	α
2.0	2.0	0.09	0.075	5.9

meantime, only a small and negligible error occurs. For an incompressible flow, Eq. (3) can be shown as the following vector:

$$\rho \frac{D\vec{D}}{Dt} = -\nabla P + B + \mu \nabla^2 \mathbf{U}. \tag{3}$$

For turbulent flows, the velocity and pressure variables are completely dependent on time; now, if we want to use them as two average and fluctuating components in the Navier-Stokes equations, a series of unknown parameters appear in the equation, which are called Reynolds stresses. By substituting the separated velocity and pressure in the Navier-Stokes equation and simplifying it, Eq. (3) becomes:

$$\rho \left(\frac{\partial \bar{u}_i}{\partial t} + \bar{u}_j \frac{\partial \bar{u}_i}{\partial x_j} \right) = \bar{B}_i - \frac{\partial \bar{P}}{\partial x_i} + \frac{\partial}{\partial x_j} \left[\mu \left(\frac{\partial \bar{u}_i}{\partial x_j} - \rho \overline{u_i' u_j'} \right) \right]. \tag{4}$$

The difference between the resulting momentum equation and the instantaneous momentum equation is the last term on the right side of Eq. (4), which is called the Reynolds stress or disturbance stress. It is more suitable for simulating the flow behavior near the wall at low Reynolds numbers and separating the flows caused by the reverse pressure gradient compared to the k-ϵ model. Unlike the k-ϵ model, which incorporates nonlinear and complex damping functions, the k-ω model offers a simplified approach by neglecting these terms. The k-ω turbulence model posits a direct relationship between turbulent viscosity, turbulent kinetic energy, and turbulence frequency. In the k-ω model, the turbulence viscosity is obtained from the following Eq. (5):

$$\mu_t = \frac{\rho k}{\omega}. \tag{5}$$

The two transfer equations of this model, the turbulent kinetic energy equation (k) and the specific dissipation rate equation (ω) are as given in Eqs. (6) and (7), respectively.

$$\frac{\partial(\rho k)}{\partial t} + \nabla \cdot (\rho U k) = \nabla \cdot \left[\left(\mu + \frac{\mu_t}{\sigma_k} \right) \nabla k \right] + P_k + P_{kb} - Y_k, \tag{6}$$

$$\frac{\partial(\rho \omega)}{\partial t} + \nabla \cdot (\rho U \omega) = \nabla \cdot \left[\left(\mu + \frac{\mu_t}{\sigma_\omega} \right) \nabla \omega \right] + \alpha \frac{\omega}{k} P_k + P_{\omega b} - Y_\omega. \tag{7}$$

The constants of this equation are shown in Table 1.

The constants in the k-ω turbulence model (Table 1) were validated through comparison with experimental data and established benchmarks for turbulent flows. These constants were derived from extensive empirical studies and are widely accepted in the literature for simulating wall-bounded flows with adverse pressure gradients. The model's accuracy was further verified by comparing simulation results with experimental measurements of velocity profiles and turbulence statistics in similar geometries.

The capacity of standard two-equation turbulence models to accurately predict the inception and extent of flow separation from smooth surfaces under adverse pressure gradients is limited. The starting point for the development of the shear stress transfer turbulence model was the need for accurate calculations of flows with separation phenomena and reverse pressure gradients. For a long time, turbulence models were unable to account for these flows.

The k-ϵ turbulence model exhibits limitations in accurately capturing near-wall turbulent boundary layer behavior. In this region, the k-ω model offers superior performance and is more suitable for flows with adverse pressure gradients. On the other hand, the k-ω model's sensitivity to free-stream conditions outside the boundary layer can hinder its application in flows involving separation induced by pressure gradients. This sensitivity in the free stream in turbulence modeling prevents the wide substitution of ω equations in place of standard ϵ equations. This is the basis for the development of the k-ω SST (Shear Stress Transport) model, which is given in Eqs. (8) and (9) below [20].

$$\frac{\partial}{\partial t}(\rho k) + \frac{\partial}{\partial x_i}(\rho k u_i) = \frac{\partial}{\partial x_i}\left(\Gamma_k \frac{\partial k}{\partial x_j}\right) + G_k - Y_k + S_k, \tag{8}$$

$$\frac{\partial}{\partial t}(\rho \omega) + \frac{\partial}{\partial x_i}(\rho \omega u_i) = \frac{\partial}{\partial x_i}\left(\Gamma_\omega \frac{\partial \omega}{\partial x_j}\right) + G_\omega - Y_\omega + D_\omega + S_\omega. \tag{9}$$

In the standard k-ω and SST k-ω models, the production terms of the k and ω equations are dissected presented in tabular form in Table 2 below.

Table 2. Terms in the $k-\omega$ turbulence model

Term	**Standard k-ω equation**	**SST k-ω equation**
Production of k	$P_k = \tau_{ij}\frac{\partial U_i}{\partial x_j} = \nu_t S_{ij} S_{ij}$	$G_k = \tau_{ij}\frac{\partial U_i}{\partial x_j}$
Buoyancy production of k	$P_{kb} = -\frac{g_i}{\rho}\frac{\partial \rho}{\partial x_i}$	
Production of ω	$P_\omega = \alpha \frac{\omega}{k} P_k$	$G_\omega = \frac{\gamma}{\nu_t} G_k$
Buoyancy production of ω	$P_{\omega b} = C_{\omega b}\frac{\omega}{k} P_{kb}$	
Dissipation of k	$Y_k = \beta^* \rho k \omega$	
Dissipation of ω	$Y_\omega = \beta \rho \omega^2$	
Cross-diffusion	Not present	$D_\omega = 2(1-F_1)\rho\sigma_{\omega 2}\frac{1}{\omega}\frac{\partial k}{\partial x_i}\frac{\partial \omega}{\partial x_i}$
Source terms	Not present	$S_k = C_k \rho \frac{\lvert S\rvert^3}{\omega}$ $S_\omega = C_\omega \rho \lvert S\rvert^2$

Turbulence models such as k-ϵ or LES are less accurate for near-wall flow behavior and need more computation workload, but the k-ω SST model combines the strengths of the k-ϵ model for free shear flows and the k-ω model for near-wall flows and thus strikes a balance between accuracy and computational efficiency. The k-ω SST turbulence model is well-known for its success in simulating turbulent flows in structures containing complex geometries and boundary layers by accurately resolving the boundary layer and near-wall flow behavior, which is essential for calculating WSS and other hemodynamic parameters [21, 22].

Studies have shown that the k-ω SST model provides accurate estimates of wall shear stress and flow separation, which are critical parameters in cardiovascular health assessment [22]. The application of these models in pulsatile flow simulations has also been validated through comparisons with experimental data. For example, the k-ω SST model has been shown to provide

highly accurate results, usually within 5% error, when compared to experimental measurements [23]. As a result, the k-ω SST turbulence model was chosen for this study due to its superior performance and for being a validated and reliable choice for simulating blood flow in stenotic vessels. The Carreau-Yasuda model, which takes into account the shear thinning properties of blood that become important under variable flow conditions [22, 24], has been widely used for simulating pulsating blood flow, and has been supported by studies to be an effective model in capturing the complex flow properties observed in biological systems [21, 22]. Furthermore, integrating the Carreau-Yasuda model with the k-ω SST turbulence model provides a more comprehensive understanding of flow dynamics in occluded arteries because it effectively captures both the non-Newtonian properties of blood and the turbulent flow characteristics [22–24].

In the present study, blood has a profile similar to that in the study of Chen and Lu [25] and enters the inlet branch at a Reynolds number equal to 270 (or an average velocity of 0.0694 m/s). As for the output boundary conditions, zero relative pressure at the outlet of the two branches is used, as per the above study, and due to the incompressibility of blood in this problem, the amount of working pressure does not affect the results. Additionally, the axial flow velocity gradients at the exits of both branches are considered to be zero. The boundary condition of the wall is assumed to be non-slip. In the present study, blood flow in a bifurcating blood vessel has been numerically

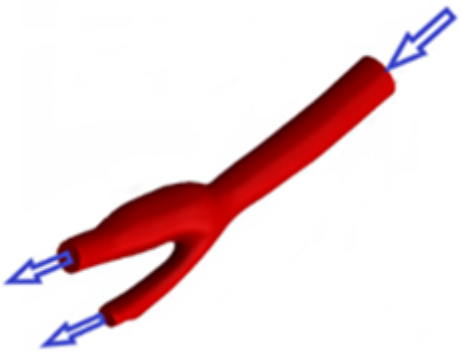

Figure 1. Blood vessel geometry

simulated in a three-dimensional model for Newtonian and non-Newtonian Carreau–Yasuda viscosity conditions. The desired geometry is drawn in the design software. Figure 1 shows the geometry drawn in SOLIDWORKS software. The Carreau-Yasuda model has been chosen for this study due to its ability to accurately describe the shear-thinning behavior of blood across a wide range of shear rates. Unlike the power-law model, which is limited to intermediate shear rates, and the Casson model, which does not account for the gradual transition between Newtonian and non-Newtonian behavior, the Carreau-Yasuda model captures the viscosity variation of blood more comprehensively. This makes it particularly suitable for simulating blood flow in vessels with complex geometries and varying shear conditions.

The shear thinning behavior of blood is described by the Carreau-Yasuda model using:

$$\mu(\dot{\gamma}) = \mu_\infty + (\mu_0 - \mu_\infty)\left[1 + (\lambda\dot{\gamma})^a\right]^{\frac{n-1}{a}},$$

where $\mu(\dot{\gamma})$ is the dynamic viscosity as a function of shear rate (γ), μ_0 is the zero-shear viscosity, μ_∞ is the infinite-shear viscosity, λ is the relaxation time, n is the power-law index that describes the degree of shear thinning, and a is the Yasuda parameter that controls the transition between Newtonian and shear-thinning regions. Values of these model parameters are presented in Table 3.

The heartbeat pattern has been selected as the pulse function, and because the Fluent software is not able to define this type of pulse, the custom codes have been defined to induce the pulse for the simulation and have been incorporated into the solver through the use of UDFs. To simulate pulsatile blood flow in a CFD model, a physiological waveform that represents the heartbeat has been obtained by using a Fourier series to approximate the periodic nature of the arterial pulse. The blood flow rate calculated based on the waveform derived from experimental data or idealized representations of the cardiac cycle has been represented by the following formula:

$$Q(t) = Q_{\text{mean}} + \sum_{n=1}^{N} \left[A_n \cos\left(\frac{2\pi nt}{T}\right) + B_n \sin\left(\frac{2\pi nt}{T}\right) \right]. \tag{10}$$

In Eq. (10), the wave function can also be converted into a single sinusoidal form by using amplitudes and phase-shift:

$$A_n \cos\left(\frac{2\pi nt}{T}\right) + B_n \sin\left(\frac{2\pi nt}{T}\right) = C_n \sin\left(\frac{2\pi nt}{T} + \phi_n\right),$$

where the amplitude $\mathbf{C_n}$ is:

$$C_n = \sqrt{A_n^2 + B_n^2}.$$

And the phase angle ϕ_n is:

$$\phi_n = \tan^{-1}\left(\frac{A_n}{B_n}\right).$$

Eq. (10), then becomes:

$$Q(t) = Q_{\text{mean}} + \sum_{n=1}^{N} C_n \sin\left(\frac{2\pi nt}{T} + \phi_n\right),$$

where T is the period of the cardiac cycle (typically 0.8–1.0 s for a heart rate of 60–75 bpm), ϕ_n are the phase angles for each harmonic, N is the number of harmonics (typically 4–10 for a realistic waveform). The parameters and respective values used to simulate the pulse are presented in Table 3 below.

With the given parameters, the pulsatile blood flow has been simulated in the modeled vessel. The Womersley number, which characterizes the pulsatile blood flow, has been calculated for the non-stenotic and stenotic (%50 and %80 constricted) cases using:

$$\alpha = \frac{r\sqrt{\omega\rho}}{\mu},$$

and respective α numbers were found to be 52.46, 26.23, and 10.49, respectively.

The solution domain is organized and discretized using the so-called O-shaped mesh, except near the tip of the bifurcation and that part of the outlet branch that includes the constriction. Additionally, the unorganized mesh adapts better to the mix of the flow (caused by the presence of bifurcations and obstructions). Therefore, in this area, an unorganized mesh has been used in a

Table 3. Parameters used to simulate the pulsatile blood flow

Property	Value(s)
Vessel diamater	0.0045 m
Density	1060 kg/m3
Zero-shear viscosity	0.056 Pa.s
Infinite-shear Viscosity	0.0035 Pa.s
Temperature	37 C
Mean velocity	0.0694 m/s (Re=270)
Period of cardiac cycle	1 s
Number of harmonics	5
Cosine coefficients (B_n)	0.2, 0.15, 0.1, 0.05, 0.02
Sine coefficients (A_n)	0.3, -0.1, 0.08, -0.03, 0.015
Amplitudes (C_n)	0.36, 0.18, 0.13, 0.058, 0.025
Phase Angles (ϕ_n, radian)	0.59, -0.59, 0.67, -0.54, 0.64
Power-law index (n)	0.03568
Yasuda parameter (a)	2
Relaxation time (λ)	3.313 s

small enough way. Ansys Fluent software, which can create unorganized and organized meshes, was used to create the mesh, which can be seen in Figure 2 below. The number of generated mesh was 122540 elements. To determine the correct number of elements to build the mesh, a mesh independence analysis was made, and convergence was established.

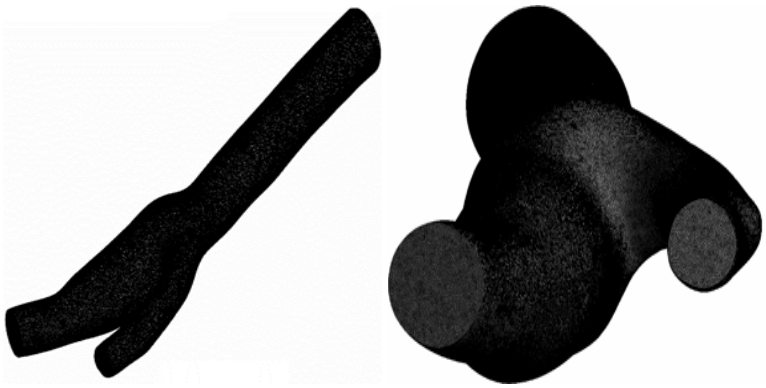

Figure 2. Side and front views of the meshed model

For numerical analysis in the ANSYS Fluent software, it is necessary to provide boundary conditions. To model the inlet flow, the mass flow rate values given in the reference study have been used. The outlet pressure boundary condition has been used for both of the two outlets of the artery division. Since the solution is unsteady, a user-defined function is used to provide the input and output boundary conditions. Figure 3 shows a view of the desired geometry along with the boundary conditions, and Figure 4 shows the values for the input and output blood pressure as given by the reference study.

In order to ensure that the number of elements that constitute the mesh have no or negligible impact on the solution, a mesh independence test is always carried out. In this study, mesh independence was demonstrated using WSS values. WSS is a critical parameter in hemodynamic simulations and is highly sensitive to mesh resolution. Therefore, it is often the primary metric for mesh independence. Once WSS converges with mesh refinement, it implicitly means that the mesh is also validated for the accuracy of velocity and pressure fields, as these are the underlying

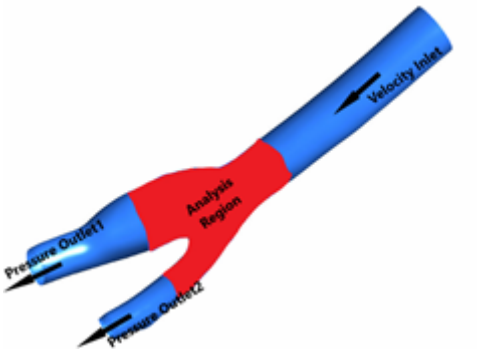

Figure 3. Boundary conditions of blood vessel geometry

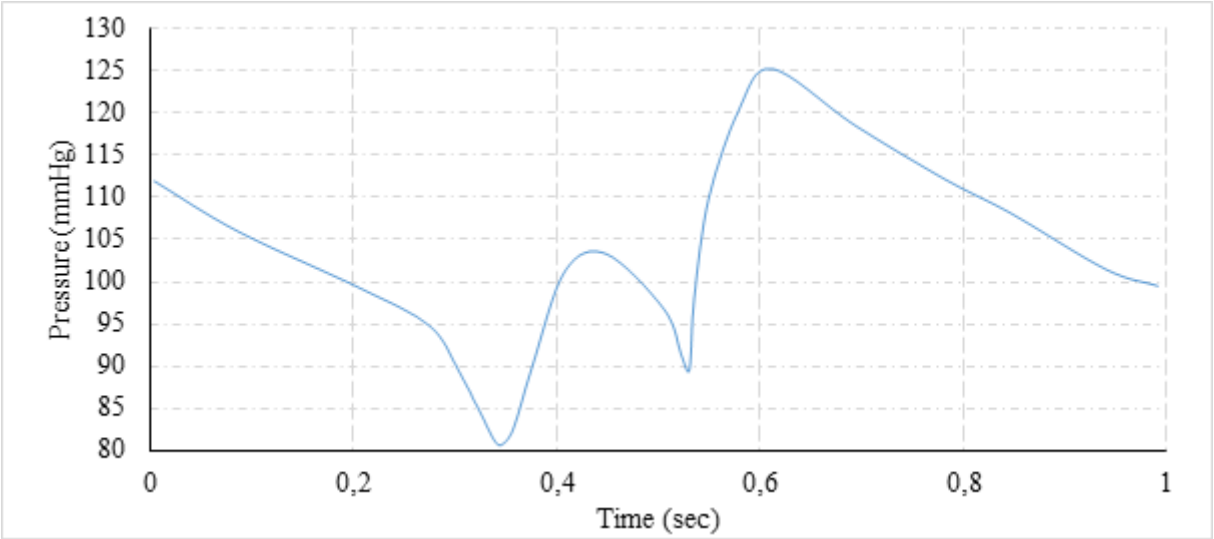

Figure 4. Input and output values of blood flow according to time

quantities used to compute WSS. In this regard, the WSS parameter in a section near the wall has been investigated in meshes with different numbers of elements. As shown in Figure 5, a number of elements greater than 1350,000 inside the geometry indicates the independence of the mesh.

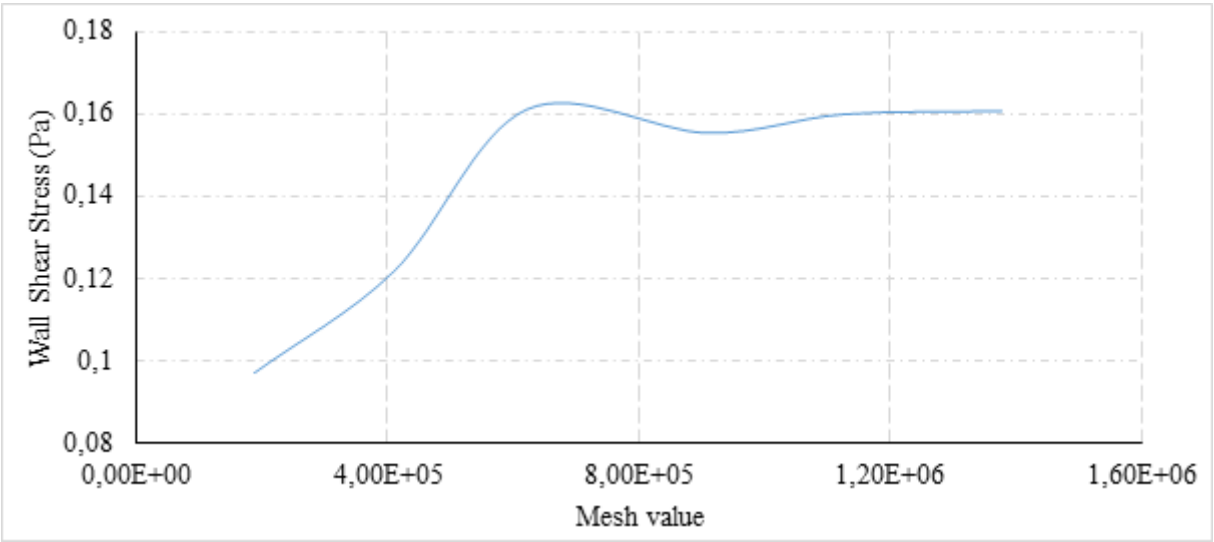

Figure 5. Shear stress according to the number of elements

One of the critical aspects of turbulence modeling is the accurate representation of near-wall flow physics, i.e., reflecting real-world conditions accurately. The performance of turbulence models is significantly influenced by their ability to capture wall-bounded flow characteristics. In this regard, the y+ parameter, a non-dimensional wall distance, serves as a crucial metric for evaluating the adequacy of near-wall mesh resolution. The logarithmic law of the wall provides theoretical guidelines for the appropriate range of y+ values to ensure accurate representation of the boundary layer. Ansys-Fluent software can be used to solve flow models that include moving cells. Depending on the complexity of movement and physics, the flow of one of the mesh movement models can be suitable for modeling. One of the most common models in Fluent for simulating streams that have a moving and variable mesh is the dynamic mesh model. To use the dynamic mesh model, we need to start with a mesh volume and describe each moving area in the model. Fluent can describe motion under a boundary profile based on functions defined by the user, known as user-defined functions (UDFs). For dynamic meshes, remeshing and smoothing techniques were employed to maintain mesh quality during deformation. Remeshing involves locally refining or coarsening the mesh in response to changes in geometry, whereas smoothing is the adjustment of nodes' positions to reduce distortion. These techniques ensure accurate simulation of fluid-structure interactions and moving boundaries.

3 Results and discussion

Many models have been presented to simulate non-Newtonian blood fluid in vessels, but none of them have been able to analyze the elastic behavior of vessel walls due to the pulse pressure of the blood, as in real samples, to minimize deviation. This problem has become one of the reasons for the failure of researchers. Computer simulation can solve the most complex problems of engineering sciences; therefore, in such problems, all required algorithms are simulated according to real vessel samples. The geometry of the vessel, which includes a two-way vessel with a diameter of the outlet different from the diameter of the inlet, is drawn, tested, and compared in the region before the constriction with different percentages. To create more tension in the vessel and complicate the problem, the diameter of one of the outlets is reduced by half, and the results are compared with each other. This complexity enables us to solve similar problems and analyze the output information. Different models are available to define blood fluid in the software. The selected models include three models: a non-Newtonian power law, a Newtonian power law, and the Carreau model, which has the least error compared to the analytical solution.

WSS (τ_w) is calculated from the velocity gradients on the wall of the vessel using the following relationship:

$$\tau_w = \mu \left(\frac{\partial u}{\partial y} \right)_{y=0},$$

where μ is the dynamic viscosity of blood, u is the velocity parallel to the wall, and y is the distance perpendicular to the wall. ANSYS uses the same formulation to calculate the wall stress based on the velocity gradients obtained during the numerical solution of the governing Navier-Stokes equations at the wall (y=0). In this study, the contour plots for WSS were obtained directly in CFD post and presented in Figure 6 for different conditions.

The shear stress values obtained in this simulation were validated against those of another study conducted using a similar bifurcation vessel model. The values are presented in Table 4. The range of the errors is from approximately 2 to 13%, and the average error is approximately 7%, which is acceptable. Figure 6 shows the distribution of inner-wall shear stress.

The results of the analysis are given as shear stress values near the vessel wall. Figure 6 shows

Table 4. Inner wall shear stress

X/C Time (s)	Shear Stress (Pas) CFD (A)	Shear Stress (Pas) [16] (B)	Error (%) (B-A)/A*100
0.0	0.123	0.12	−2.5
0.2	0.174	0.18	3.4
0.4	0.280	0.26	−7.1
0.6	0.355	0.38	7.0
0.8	0.220	0.24	9.0
1.0	0.150	0.13	−13.3

the values of shear stress inside the vessel resulting from the analysis with the Carreau model. The average value near the vessel wall is approximately 0.3 Pascal. In the case of constriction, the region behind the constriction experiences the highest shear stress. The flow output also has shear stress values, and this stress increases with the narrowing of the outlet of the vessel.

Figure 6 show shear stress values on walls of the vessel with 80% and 50% constriction. The shear stress is highest in the region near the branch and near the constriction because of the increase in pressure in these areas. With the narrowing of the constriction due to a sudden change in diameter, the velocity in the narrowed channel increases greatly, which in turn increases the pressure on the wall, and with the narrowing of the outlet, this pressure increases. The tension at these points increases due to the increase in pressure. The concentration of greatest stress occurs after constriction and in the furcation area.

The velocity streamlines in Figure 7 show that the flow characteristics in normal and stenotic arteries change significantly. While the velocity distribution in the normal artery is relatively balanced, the flow lines progress smoothly, and no significant recirculation or turbulence is observed. With the increase of constriction, a significant increase in the flow velocity and the formation of turbulence in the region after the constriction are observed with the expansion of backflow areas. This supports the formation of high shear stresses in the arterial wall seen in Figure 6.

Figure 8 shows the values of the velocity inside the vessel for different modes of analysis. As it approaches the area before the constriction, due to the increase in pressure, the flow experiences a sharp drop in velocity, which acts like the flow inside the nozzle in the constriction area, and a higher velocity is observed in the flow of the constriction area. This increase in velocity continues to the furcation area, which induces an increase in friction and shear stress. In the case where the outlet of the vessel is narrowed, the increase in velocity increases, and up to 17% greater velocity is observed in the furcation area. With increasing velocity, the amount of pressure and shear stress increases, and the vessel is unable to bear this pressure and is on the threshold of rupture.

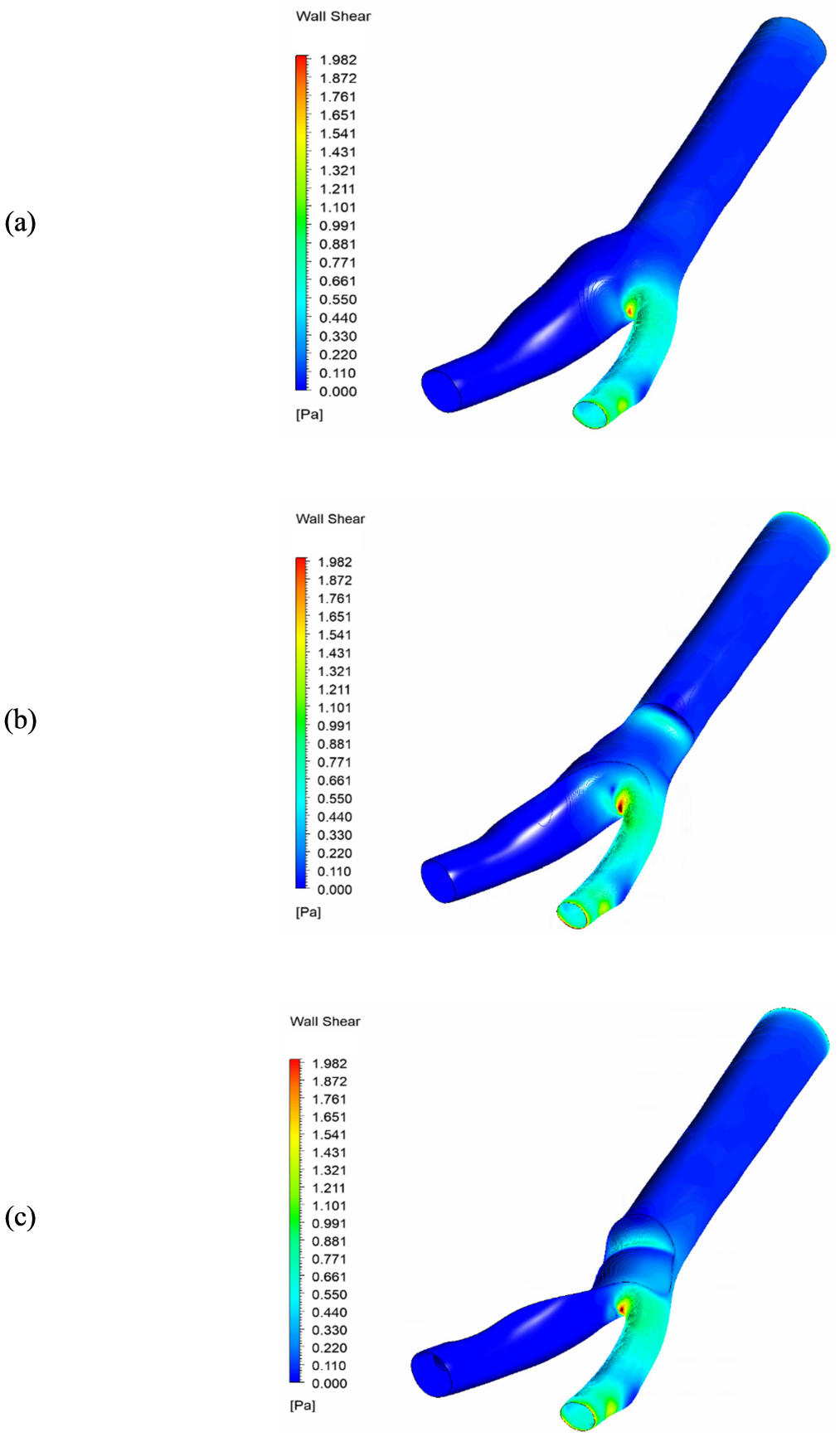

Figure 6. Shear stress contours on (a) normal (b) 50% and (c) 80% constricted vessel

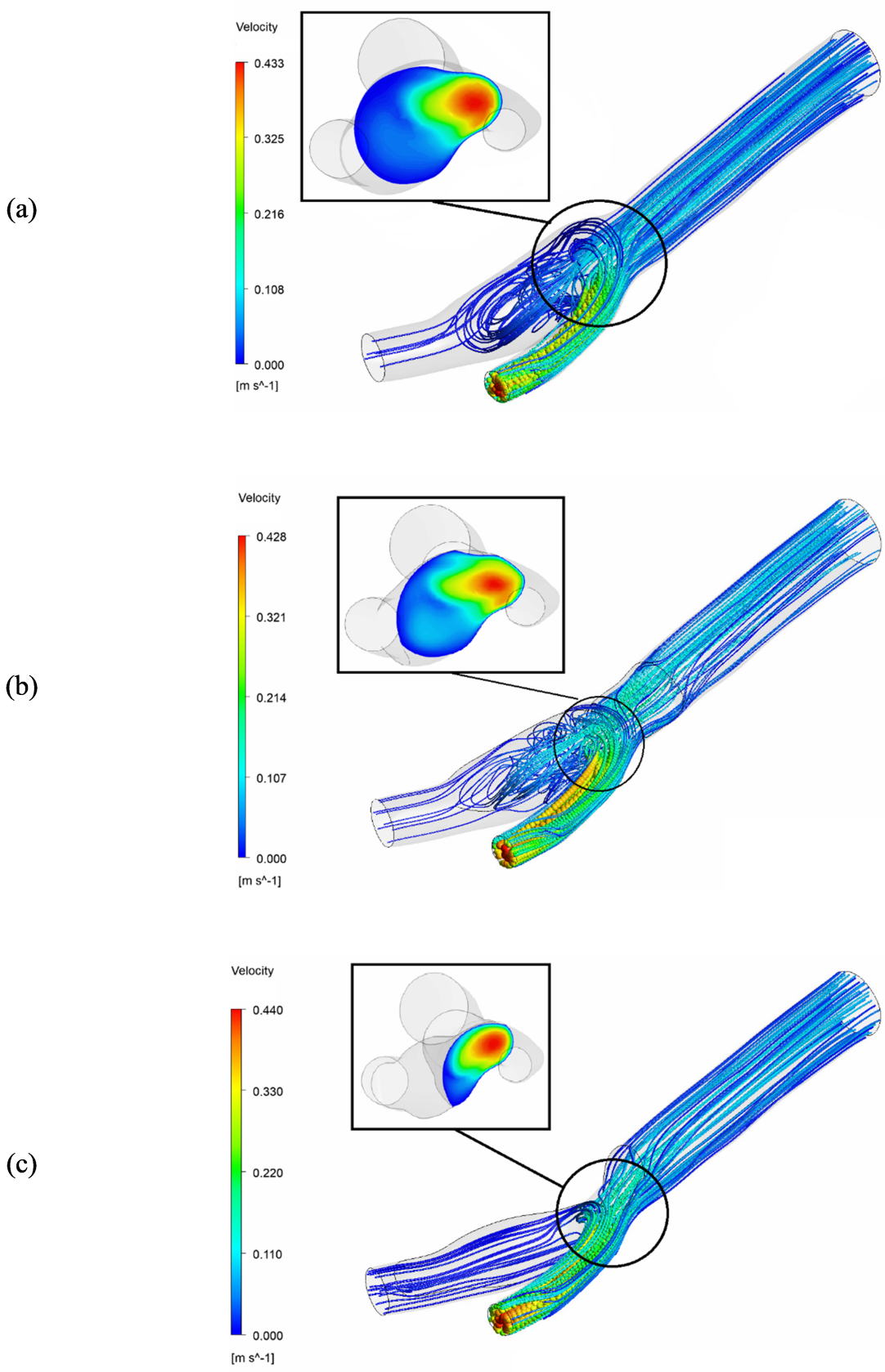

Figure 7. Velocity values of vessel geometry (a) normal (b) 50% and (c) 80% constricted vessel

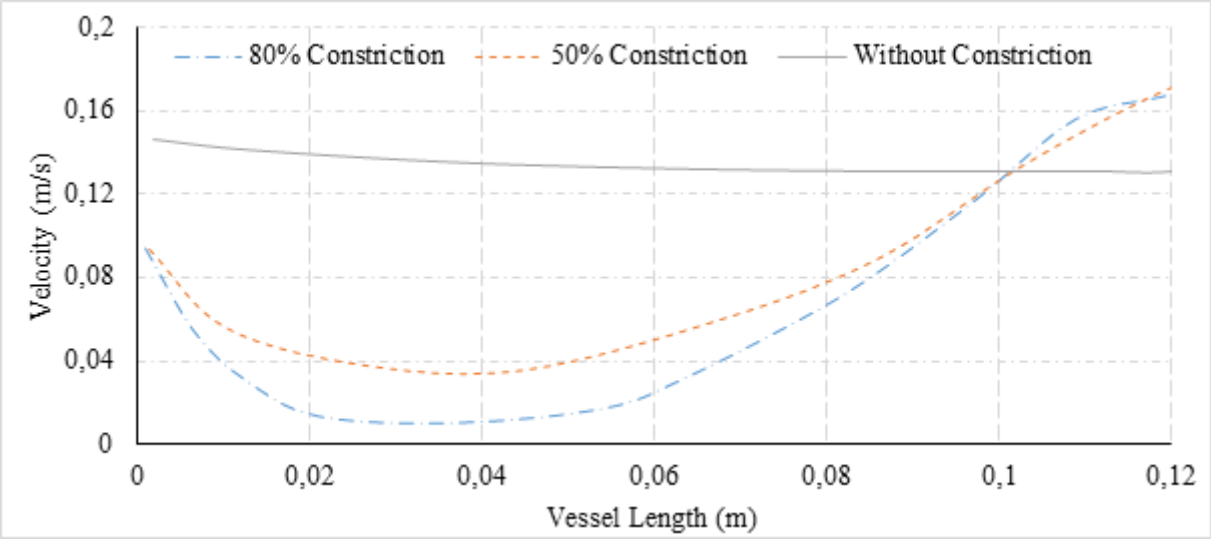

Figure 8. Velocity values before the furcation for different conditions

As seen from the pressure values, the effect of pressure is also evident within the entire tissue of the vessel wall. The shear stress values of the wall grid due to this pressure are given in Figure 9. In this case, the wall tissue will not bear this pressure and will be on the verge of tearing. As seen from the deformation values, the effect of pressure inside the tissue of the vessel wall is also evident; with the increase in the amount of relaxation, the pressure increases. In Figure 10,

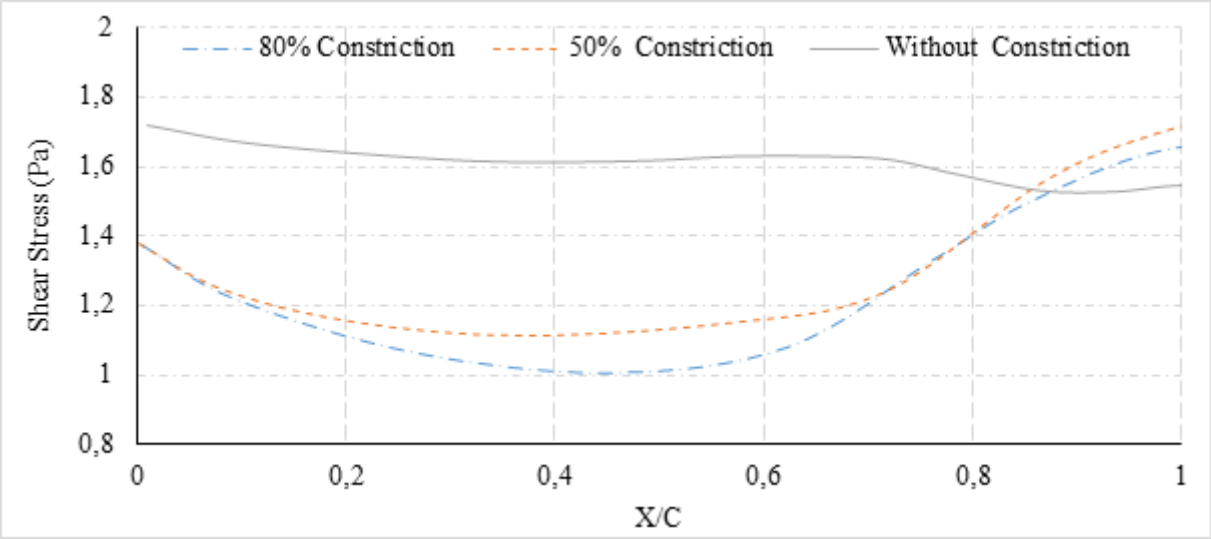

Figure 9. Shear stress values before the flow crossroads on the wall for different

the pressure values inside the vessel are analyzed for different states. By approaching the area before the constriction, due to the increase in pressure, the flow encounters an increase in pressure, which acts like the flow inside the nozzle in the constriction area, and more pressure is observed in the flow of the constriction area. This increase in pressure continues to the furcation area, which causes an increase in friction and shear stress. In the case where the outlet of the vessel is narrowed, this increase in pressure is greater. Shear stress is a critical factor in the development of thrombosis. Low shear stress (< 0.4 Pa) promotes platelet adhesion, whereas high shear stress (> 1.0 Pa) potentially causes endothelial damage. The shear stress values observed in this study, particularly near occlusions, fall within these clinically relevant ranges.

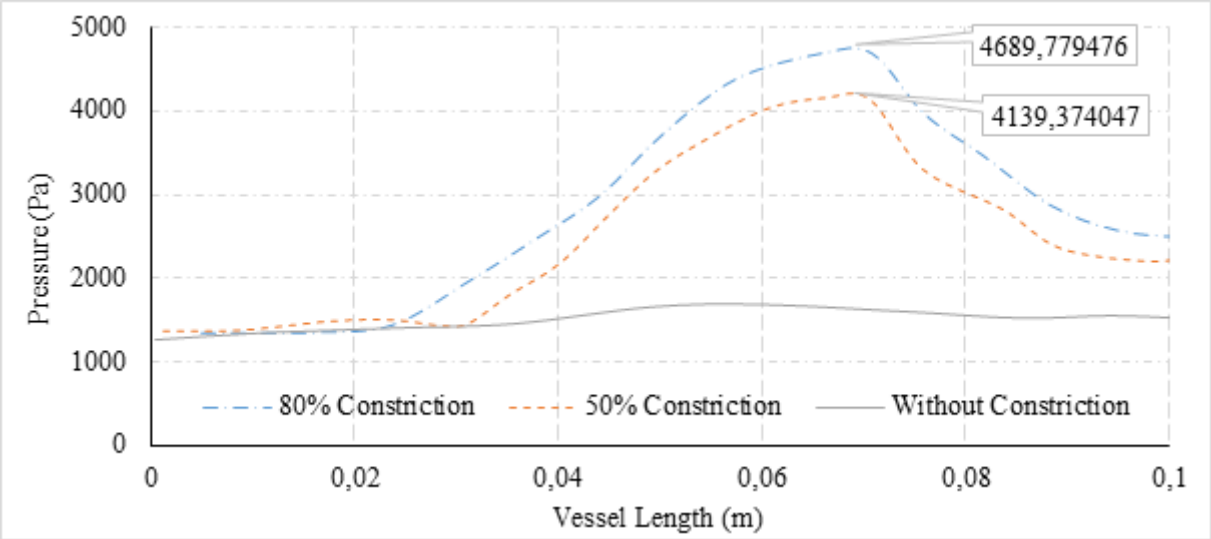

Figure 10. Velocity values before the furcation for different conditions

When the highest pressure values near the occlusions are concerned, the maximum pressure was found to be 4139,37 Pa for the 50% constriction case, it reached 4689,78 Pa for the 80% constriction case. These elevated pressure values highlight the increased risk of vessel wall damage in highly occluded vessels. The pressure values suggest that the occlusion exerts pressure on the entire vessel wall, clearly indicating that clogging causes a sharp pressure increase in the vessel just before the stenosis.

4 Conclusion

The stress–strain relationship in the blood does not follow a single relationship. This analysis depends on the dimensions of the vessel compared to the dimensions of the particles present in plasma (red and white blood cells, and platelets). The behavior of blood flow in vessels with a large internal diameter adheres to well-established hemodynamic principles, where inertial forces dominate viscous forces, and the continuum assumption remains valid. To achieve the objectives of the research, the numerical studies carried out in this field are first discussed, and in this part, the main focus has been on the research carried out using Ansys software. In the second part, the computational studies performed on the blood flow are discussed, and then the governing equations are explained. Furthermore, the vessel model was selected from reliable sources to ensure the validity of the simulation data. The results indicate the approximate accuracy of the non-Newtonian model used. Continuing this research, vessel occlusion models with varying occlusion sizes have been analyzed. The effect of pressure on the vessel wall tissue is evident. For small occlusions, large vessels can withstand the pressure. Although the software cannot simulate rupture, the vessel wall tissue appears capable of tolerating up to 50% stenosis.

In a vessel with 80% constriction of the internal diameter and a narrowed outlet, pressure values indicate high pressure intensity and velocity heterogeneity. This leads to a significant increase in shear stress near the constriction while the vessel flow exerts pressure on the wall. Wall mesh deformation due to this pressure suggests that the wall tissue would not withstand this level of pressure and would be at the threshold of tearing.

Velocity values within the vessel are analyzed under different conditions. As the flow approaches the constricted area, velocity sharply decreases due to increased pressure. Within the constriction, the flow behaves similarly to that inside a nozzle, resulting in higher fluid velocity in the narrowed region of the vessel.

This study highlights the importance of accurately modeling non-Newtonian blood behavior and vessel occlusion to understand the hemodynamic risk factors associated with CVDs.
The main findings of the study can be summarized as follows:

- It was observed that blood modeled as a non-Newtonian fluid exhibited significant differences in flow patterns compared to the Newtonian assumption and that the Carreau-Yasuda model played a critical role in determining the flow dynamics in high shear stress regions near the stenosis.
- The fact that the maximum WSS values were significantly higher in non-Newtonian flows indicated the importance of using the Carreau-Yasuda model to consider the shear thinning behavior of blood in hemodynamic studies.
- It was observed that the narrowing of the vessel significantly changed the flow characteristics of the blood. In the case of 50% and 80% constrictions, the axial velocity in the non-planar branch decreased, while the velocity and, hence, the pressure increased in the furcation region, which led to an increase in the critical factor of wall shear stress.
- When the velocity distributions within the vessel were evaluated, it showed significant heterogeneity, especially in the regions downstream of the occlusion, which could worsen the vascular damage due to hemodynamic risk factors such as flow separation, recirculation, and turbulence.
  - The use of the k-ω SST turbulence model has been shown to provide accurate resolution of near-wall flow physics and adverse pressure gradients, which are critical for capturing complex flow patterns in narrow vessels

5 Limitations

Although this study provides valuable information on the hemodynamics of the constricted vessels, the study is limited by the fact that the viscoelastic effects of blood and vessel walls are neglected, which may affect the flow dynamics, especially in highly stenotic regions. Another limitation is that the study does not include experimental validation.

6 Future Research

To take this research further, future studies can use viscoelastic models that take into account the elastic behavior of blood and vessel walls. Numerical results can be validated with experimental data obtained by techniques such as MRI or ultrasound. The effects of different turbulence models, such as Large Eddy Simulations and Reynold Stress Model on the accuracy of hemodynamic predictions can be investigated.

Declarations

Use of AI tools

The authors declare that they have not used Artificial Intelligence (AI) tools in the creation of this article.

Data availability statement

No Data associated with the manuscript.

Ethical approval (optional)

The authors state that this research complies with ethical standards. This research does not involve either human participants or animals.

Consent for publication

Not applicable

Conflicts of interest

The authors declare that they have no conflict of interest.

Funding

No funding was received for this research.

Author's contributions

M.M.: Conceptualization, Methodology, Investigation, Data Curation, Formal Analysis, Writing-Original draft, Software, Visualization, Validation. İ.K.: Resources, Supervision, Writing-Reviewing and Editing. M.K.Y.: Methodology, Investigation, Data Curation, Formal Analysis, Validation, Writing-Original Draft, Writing-Reviewing and Editing. All authors discussed the results and contributed to the final manuscript.

Acknowledgements

Not applicable

References

[1] Pontrelli, G. Pulsatile blood flow in a pipe. *Computers & Fluids*, 27(3), 367-380, (1998). [CrossRef]

[2] Gijsen, F.J.H. *Modeling of Wall Shear Stress in Large Arteries.* Ph.D. Thesis, Technische Universiteit Eindhoven, (1998). [https://doi.org/10.6100/IR510253]

[3] Nathan, D.M. Long-term complications of diabetes mellitus. *New England Journal of Medicine*, 328(23), 1676-1685, (1993). [CrossRef]

[4] Kannel, W.B. and McGee, D.L. Diabetes and cardiovascular disease: the Framingham study. *Jama*, 241(19), 2035-2038, (1979). [CrossRef]

[5] Ishikawa, T., Guimaraes, L.F., Oshima, S. and Yamane, R. Effect of non-Newtonian property of blood on flow through a stenosed tube. *Fluid Dynamics Research*, 22, 251, (1998). [CrossRef]

[6] Nichols, W.W., O'Rourke, M., Edelman, E.R. and Vlachopoulos, C. *McDonald's Blood Flow in Arteries: Theoretical, Experimental and Clinical Principles*. CRC Press: USA, (2022). [CrossRef]

[7] Kumar, G., Kumar, H., Mandia, K., Zunaid, M., Ansari, N.A. and Husain, A. Non-Newtonian pulsatile flow through an artery with two stenosis. *Materials Today: Proceedings*, 46(20), 10793-10798, (2021). [CrossRef]

[8] Ahmed, S.A. and Giddens, D.P. Pulsatile poststenotic flow studies with laser Doppler anemometry. *Journal of Biomechanics*, 17(9), 695-705, (1984). [CrossRef]

[9] Siouffi, M., Peronneau, P., Wildt, E. and Pelissier, R. Modifications of flow patterns induced by a vascular stenosis. In Proceedings, *of Euromech*, pp. 73-88, Paris, France, (1977, November).

[10] Tu, C., Deville, M., Dheur, L. and Vanderschuren, L. Finite element simulation of pulsatile flow through arterial stenosis. *Journal of Biomechanics*, 25(10), 1141-1152, (1992). [CrossRef]

[11] Marshall, I., Zhao, S., Papathanasopoulou, P., Hoskins, P. and Xu, X.Y. MRI and CFD studies of pulsatile flow in healthy and stenosed carotid bifurcation models. *Journal of Biomechanics*, 37(5), 679-687, (2004). [CrossRef]

[12] Steinman, D.A., Thomas, J.B., Ladak, H.M., Milner, J.S., Rutt, B.K. and Spence, J.D. Reconstruction of carotid bifurcation hemodynamics and wall thickness using computational fluid dynamics and MRI. *Magnetic Resonance in Medicine*, 47(1), 149-159, (2002). [CrossRef]

[13] Seo, T. Hemodynamic characteristics in the human Carreautid artery model induced by blood-arterial wall interactions. *International Journal of Biomedical and Biological Engineering*, 7(5), 153-158, (2013).

[14] Biswas, D. and Laskar, R.B. Steady flow of blood through a stenosed artery: A non-Newtonian fluid model. *Assam University Journal of Science & Technology: Physical Sciences and Technology*, 7(2), 144-153, (2011).

[15] Chaichana, T., Sun, Z. and Jewkes, J. Computation of hemodynamics in the left coronary artery with variable angulations. *Journal of Biomechanics*, 44(10), 1869-1878, (2011). [CrossRef]

[16] Dong, J., Sun, Z., Inthavong, K. and Tu, J. Fluid-structure interaction analysis of representative left coronary artery models with different angulations. In Proceedings, *Computing in Cardiology 2013*, pp. 5-8, Zaragoza, Spain, (2013, September).

[17] Van Leeuwen-van Zaane, F., de Bruijn, H.S., Sterenborg, H.J.M.C. and Robinson, D.J. The effect of fluence rate on the acute response of vessel diameter and red blood cell velocity during topical 5-aminolevulinic acid photodynamic therapy. *Photodiagnosis and Photodynamic Therapy*, 11(2), 71-81, (2014). [CrossRef]

[18] Botti, L., Paliwal, N., Conti, P., Antiga, L. and Meng, H. Modeling hemodynamics in intracranial aneurysms: Comparing accuracy of CFD solvers based on finite element and finite volume schemes. *International Journal for Numerical Methods in Biomedical Engineering*, 34(9), e3111, (2018). [CrossRef]

[19] Eum, T.S., Seo, I.W., Shin, E.T. and Song, C.G. Development and application of a user-friendly general-purpose predictive simulation tool for two-dimensional flow analysis. *Environmental Modelling & Software*, 163, 105665, (2023). [CrossRef]

[20] La Porta, G., Leonardi, A., Pirulli, M., Cafaro, F. and Castelli, F. Time-resolved triggering and runout analysis of rainfall-induced shallow landslides. *Acta Geotechnica*, 19, 1873-1889, (2024). [CrossRef]

[21] Tabe, R., Ghalichi, F., Hossainpour, S. and Ghasemzadeh, K. Laminar-to-turbulence and relaminarization zones detection by simulation of low Reynolds number turbulent blood flow in large stenosed arteries. *Bio-medical Materials and Engineering*, 27(2-3), 119-129, (2016). [CrossRef]

[22] Mahalingam, A., Gawandalkar, U.U., Kini, G., Buradi, A., Araki, T., Ikeda, N. et al. Numerical analysis of the effect of turbulence transition on the hemodynamic parameters in human coronary arteries. *Cardiovascular Diagnosis and Therapy*, 6(3), 208-220, (2016). [CrossRef]

[23] Mohd Saat, F.A. and Jaworski, A.J. Numerical predictions of early stage turbulence in oscillatory flow across parallel-plate heat exchangers of a thermoacoustic system. *Applied Sciences*, 7(7), 673, (2017). [CrossRef]

[24] Carvalho, V., Rodrigues, N., Lima, R.A. and Teixeira, S.F.C.F. Modeling blood pulsatile turbulent flow in stenotic coronary arteries. *International Journal of Biology and Biomedical Engineering*, 14(22), 160-168, (2020). [CrossRef]

[25] Chen, J. and Lu, X.Y. Numerical investigation of the non-Newtonian pulsatile blood flow in a bifurcation model with a non-planar branch. *Journal of Biomechanics*, 39(5), 818-832, (2006). [CrossRef]

Mathematical Modelling and Numerical Simulation with Applications (MMNSA)
(https://dergipark.org.tr/en/pub/mmnsa)

How to cite this article: Mustafaoğlu, M., Kotçioğlu, İ. & Yeşilyurt, M.K. (2025). Numerical analysis of the three-dimensional model of pulsatile and non-Newtonian blood flow in a carotid artery with local occlusion. *Mathematical Modelling and Numerical Simulation with Applications*, 5(1), 97-116. https://doi.org/10.53391/mmnsa.1522021